Polímeros
ISSN 1678-5169 (Online)
(cc) BY
https://doi.org/10.1590/0104-1428.20230099

ORIGINAL ARTICLE

# A methodology for determination the inlet velocity in injection molding simulations

**Diego Alves de Miranda[1]*, Willian Kévin Rauber[2], Miguel Vaz Jr.[2] and Paulo Sergio Berving Zdanski[2]**

*[1]Departamento de Engenharia Mecânica, Universidade da Região de Joinville – UNIVILLE, São Bento do Sul, SC, Brasil*

*[2]Programa de Pós-graduação em Ciência e Engenharia de Materiais, Departamento de Engenharia Mecânica, Universidade do Estado de Santa Catarina – UDESC, Joinville, SC, Brasil*

**diegoalves_klx@hotmail.com*

## Abstract

The inlet velocity of thermoplastic in injection molds plays a crucial role in obtaining high-quality polymer parts and the final performance of the product. It is known that the way the polymer is injected into the mold can directly affect important properties, such as the distribution of internal stresses, the cooling rate and the formation of surface defects. However, there are injection molding machines that only control injection pressure and dosage, making it difficult to obtain the gate inlet velocity into the mold cavity. Besides, some molds have many injection channels as well as complex inlet geometries, which make a challenging task to identify the inlet velocity. This study presents numerical and experimental approaches on how to determine the entry velocity in thermoplastic injection molds. The main results showed that these methods are highly efficient and contribute to identifying the gate inlet velocity with good accuracy.

**Keywords:** *inlet velocity, injection molds, numerical/experimental methodologies.*

**How to cite:** Miranda, D. A., Rauber, W. K., Vaz Jr., M., & Zdanski, P. S. B. (2024). A methodology for determination the inlet velocity in injection molding simulations. *Polímeros: Ciência e Tecnologia*, *34*(1), e20240011. https://doi.org/10.1590/0104-1428.20230099

## 1. Introduction

The adequate choice of parameters in injection molding processes is a topic of great interest nowadays, since many products are manufactured by this process, in special components and parts for the automotive and aerospace industries. The behavior of the polymer flow during the injection molding process can be affected by multiple variables, some of which can be controlled by efficient mold design and setting of correct machine parameters[1].

One important variable that is able to change the mold injection process is the gate inlet velocity, that is the velocity of the molten polymer entering the mold cavity. This variable affects directly the quality of the injected parts and a proper control can prevent possible failures. The incorrect preset of the polymer velocity can produce defects, such as shrinkage and flow marks when using high velocities, whilst low velocities can lead to incomplete mold filling[2]. Furthermore, the gate inlet velocity also affects the cooling time (cooling rate) and polymer crystallization, influencing the molecular structure and final properties of products[3]. Such issues highlight the importance of understanding the gate inlet velocity, once this parameter is essential in injection mold design[4], primarily to maintain efficient control of injection molding processes[5] and achieve high-quality polymer parts and high performance[6].

In order to finding the best gate inlet velocity, as well as other processing parameters such as melting temperature, injection pressure and cycle time, numerical simulation plays a crucial role in injection molding processes[7]. The simulation of thermoplastic products prior to mold construction is increasingly becoming a powerful tool to predict and optimize processing performance and product quality[8]. Moreover, the greatest advantage of applying current advanced computational methods is the virtual model visualization, which shows the behavior of molten polymers, offering valuable insights to designers and engineers[9]. For example, Morak et al.[10] carried out injection molding simulations using Moldflow® to determine the best orientation of the polymeric fibers as a function of the mold geometry and injection parameters to improve the mechanical behavior of the injected parts. Based on injection molding simulation, Onken et al.[11] developed a numerical algorithm able to predict the weld line in the molten polymer flow. Gruber and Miranda[12] used SolidWorks Plastics® to simulate the heat transfer between different cooling channels and mold wall, in the process of injecting polypropylene parts, aiming to optimize the cycle time of the parts and at increasing productivity.

It is notable that numerical simulations help and contribute to the good performance of the thermoplastic injection process[13]. However, the design engineer must know how to properly set the polymer parameters and the injection process [14]. Some research works present

simulations under which the boundary conditions use inlet velocity and inlet temperature as input parameters, which are normally chosen arbitrarily[15]. For example, Young[16] applied the lattice Boltzmann method (LBM) to simulate and analyze the behavior of molten ABS and PS polymers using $100\,mm\ s^{-1}$ as gate inlet velocity. When proposing a new numerical scheme to simulate molten polymers, Zdanski and Vaz[17] used a gate inlet velocity of $60\,mm\ s^{-1}$ to simulate the POM polymer in geometries with abrupt expansions. Using the same analogy of abrupt expansions, Tutar and Karakus[18] applied three different inlet velocities to evaluate the thermophysical properties of the molten PP polymer, which were $10\,mm\,s^{-1}$, $30\,mm\,s^{-1}$ and $60\,mm\,s^{-1}$. The authors numerically analyze the flow of molten PP polymer in a free rectangular cavity and a cavity with obstruction with the objective of comparing the position of the flow front. In other work, Gao[19] used as initial inlet velocities $100\,mm\,s^{-1}$, $200\,mm\ s^{-1}$, $400\,mm\,s^{-1}$ and $2000\,mm\,s^{-1}$.

In an injection process, the flow of molten polymer is mainly controlled by the injection pressure, which in turn is established by the injection machine[20]. Molds may contain many inlet channels and gates prior to the mold cavity[21]. This mold arrangement poses some difficulties in setting the cavity entry velocity, since injection of the molten polymer requires a high pressure for the flow to occur in the channels and fill all parts[22]. In most simulations of thermoplastic injection processes, the design engineer ignores the geometry of the injection channels and gate, as this only results in more computational time, in addition to running more risks of divergences in the simulations[23]. This procedure ties the accuracy of the results with the knowledge and experience of those who set up the simulations[24]. However, there are studies that prove that, in molten polymer injection processes, depending on the gate inlet velocity, the product may suffer injection failures[25,26]. Therefore, great care must be taken to properly insert the inlet injection velocity (when such boundary conditions are preset), in order to maintain the accuracy of the results and minimize post-processing errors[27]. All aforementioned examples show that many authors arbitrary define an initial flow velocity at the entrance of the cavity or, consequently, at the exit of the gate. This is due to the fact that, in most cases, velocity is controlled at the beginning of the screw, which constitutes a considerable distance from the cavity with several section variations.

Within this context, this study proposes both experimental and numerical methods to determine the inlet velocity of thermoplastic parts processed by injection molding that have injection channels followed by a gate. Both experimental and numerical methods consist of measuring the average displacement length of the molten ABS polymer, considering a fixed injection pressure and alternating different injection times. Simulations were performed using the Generalized Hele-Shaw Approach (GHS) to predict injection molding flow characteristics of a specimen experimentally validated.

## 2. Materials and Methods

The methodology applied in this work is divided in two parts. The first one comprises experimental injection tests with specimens injected in ABS to compare the displacement length of the molten polymer for different cavity filling times. In the second step, a numerical simulation of the injection molding process of the same specimen injected in ABS is developed using the Moldflow® software.

### 2.1 Experimental procedure

The component analized in this work is a test specimen injected in acrylonitrile-butadiene-styrene (ABS 750 from Kumho Petrochemical)[28]. In addition to its widespread use in industry, the ABS 750 was used in this work owing to the experimental and numerical validation of its rheological equations performed by the authors in previous studies[24,29]. The volume of the test specimen is $8.297\,cm^3$, and the specific mass of ABS 750 is $1,033.40\,g\,cm^{-3}$ according to the material manufacturer[28], which leads to an average injected mass of $8.574\,g$. The ABS 750 was processed with an injection temperature of 235°C, a mold wall temperature of 10°C and an injection pressure of $25\,MPa$.

#### 2.1.1 Injection process

The injection mold used in the present work was manufactured in P-20 steel with only one cavity and a symmetrical bifurcation, so that the molten polymer enters the mold cavity through the sides of the test piece, as shown in Figure 1. The injection machine used in this work is the Battenfeld, model 250 Plus.

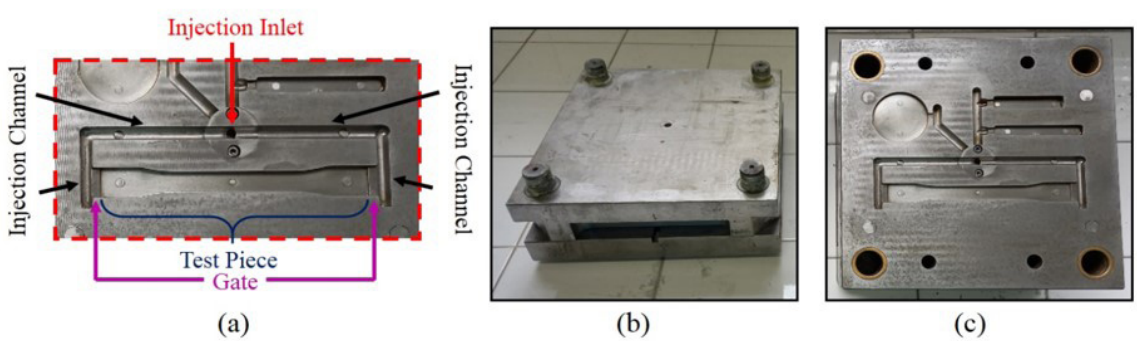


**Figure 1.** Details of the injection processing: (a) Close view of the superior Cavity; (b) Inferior cavity assemble, and (c) Superior cavity assemble.

### 2.2 Experimental determination of inlet velocity

The injection process is intermittent and composed of three main stages, namely filling, packaging and solidification, respectively. In this study, only the first stage of the injection cycle is addressed, both in experiments and simulations. Firstly, an injection pressure of $P_0 = 25\,MPa$ was used as initial processing condition. However, it is known that the pressure drop in injection channels are relatively high[30]. To ensure the accuracy of these results, the experimental method considered the injection of ten (10) different samples, which were taken from the first $\Delta t = 0.30\,s$ of injection. The displacement length of the molten polymer, referred here as filling lines ($\Delta x_{exp}$), are measured in five (5) locations along the partially injected part, from the gate, as shown in Figure 2.

From these measurements, the average length of the filling lines was determined, followed by computation of the mean velocity using Equation 1.

$$U_{0exp} = \frac{\overline{\Delta x_{exp}}}{\Delta t} \tag{1}$$

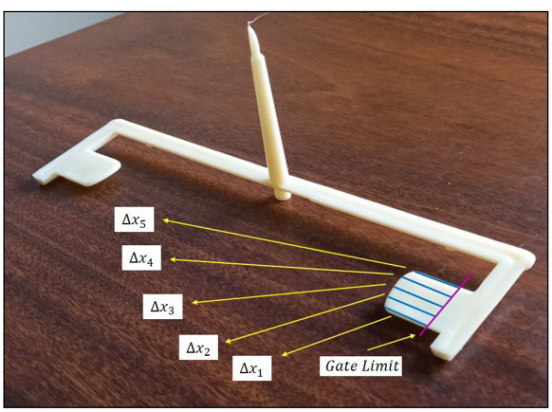


**Figure 2.** Experimental measurement process of the injected length ($\Delta x_{exp}$) at $\Delta t = 0.3\,s$.

### 2.3 Determination of inlet velocity by numerical simulation

The numerical method was also used, in which the filling lines were captured through ABS polymer simulations. Figures 3a presents the locations of the the inlet and boundary conditions, whereas Figure 3b illustrates the filling lines. The Moldflow® Adviser software was used to simulate the molten polymer injection process. Moldflow® uses the generalized Hele-Shaw model (GHS) to calculate the non-Newtonian polymer flow[31]. The initial conditions were the same used in the experiments: $P_0 = 25\,MPa$, $T_0 = 235\,℃$ and $T_w = 10\,℃$.

The filling lines were obtained for the same experimental distances, as indicated in Figure 3b. The numerical velocity based on the average filling lines are computed using Equation 2,

$$U_{0sim} = \frac{\overline{\Delta x_{sim}}}{\Delta t} \tag{2}$$

#### 2.3.1 Generalized hele-shaw model

The Moldflow® Advisor software simulates the flow of the molten polymer considering a non-Newtonian and compressible fluid under non-isothermal conditions. For more detailed clarification on the governing equations for the conservation of mass, momentum and energy for molten polymer flow, the reader is referred to Kennedy's work[31] for more details on the GHS mathematical approach and Miranda et al.[29] for further details of the thermophysical properties used in the simulations.

The interface description method for capturing the flow front used by the software is VOF (Volume of Fluid), and the method for time discretization uses an explicit Euler scheme with second-order precision. The VOF methodology is a method for capturing the boundary that can consider more than one phase. The software considers linear correlations to estimate the viscosity and density at the interface between the molten polymer and the air confined inside the mold[32]: The reader is referred to Hétu et al.[32] and Miranda et al.[29] for more details on the VOF methodology.

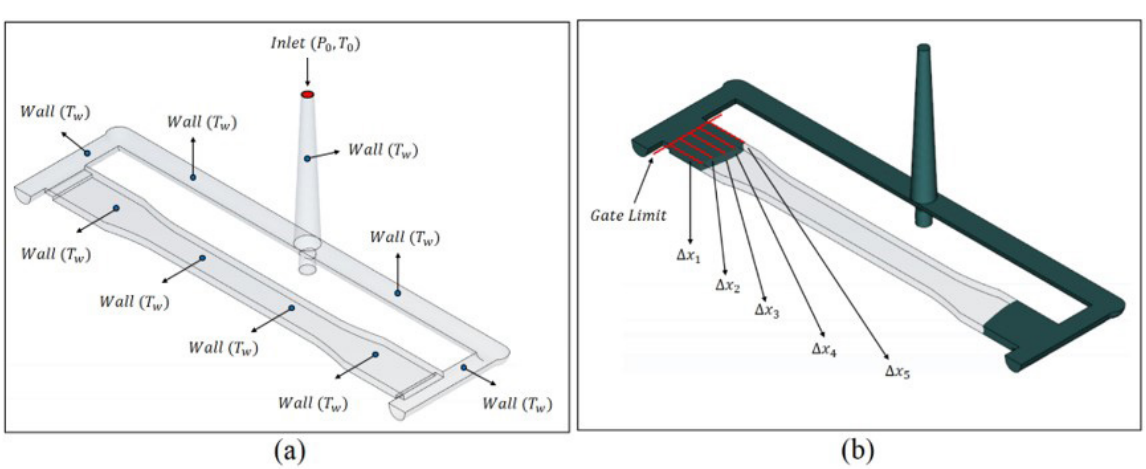


**Figure 3.** Determination of the injected length at $\Delta t = 0.3\,s$. (a) Boundary conditions of simulations with the Generalized Hele-Shaw model; (b) Simulated filling lines ($\Delta x_{sim}$).

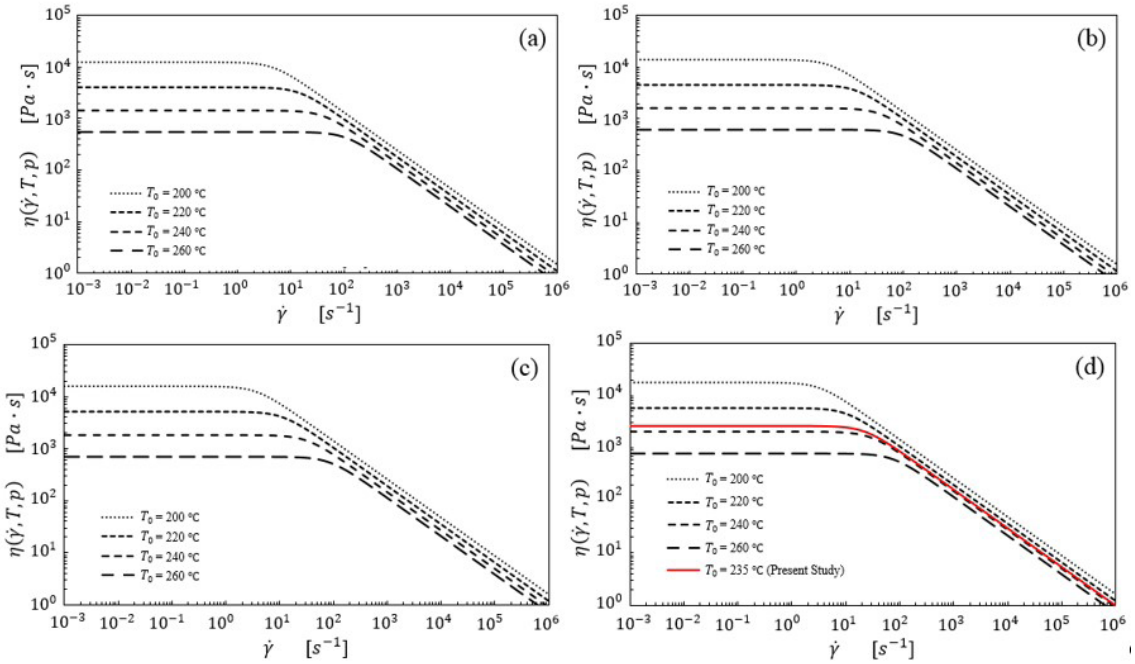


**Figure 4.** Viscosity versus shear rate in distinct injection conditions. (a) Injection pressure 10 Mpa; (b) Injection pressure 15 Mpa; (c) Injection pressure 20 Mpa; (d) Injection pressure 25 MPa.

### 2.3.2 Polymer rheology

The Moldflow® works with several viscosity models that can be used in simulations. The choice of a viscosity model must be done properly to ensure accuracy of the simulations. A previous study by Miranda et al.[29] compared several viscosity models, confronting numerical and experimental results. The authors demonstrated that the constitutive viscosity model known as Modified Arrhenius Carreau (MACa) better capture the non-Newtonian behavior of molten ABS. This model explicitly accounts for shear rate, temperature and pressure effects. For the sake of objectivity, the equations are omitted here and the reader is refeed to Miranda et al.[29] for further discussions on the effects of the rheological and processing parameters. An illustration of the effects of the shear rate, temperature and pressure in the viscosity for the molten ABS polymer is presented in Figure 4.

### 2.3.3 Numerical verification

In order to evaluate the accuracy of the ABS simulations while flowing inside the specimen cavity, a verification process was performed. Verification of transient flow proposed by Hétu et al.[32] was performed with the dimensions and boundary conditions of the domain shown in Figure 5.

Laminar flow is assumed at the inlet and no-slip boundary conditions are imposed on the cavity walls. Uniform melting temperature is set at inlet. The initial temperatures of the empty cavity and the mold wall are assumed to be the same. Finally, viscous dissipation effects were neglected. The viscosity model used by Hétu et al.[32] in the simulation is the modified Arrhenius Bird–Carreau model

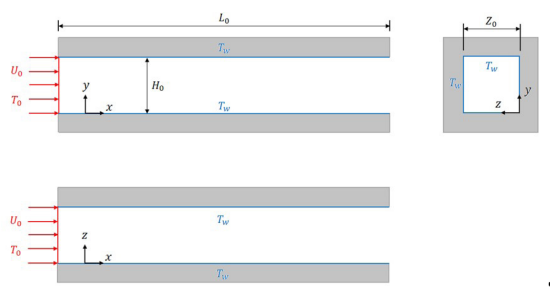


**Figure 5.** Boundary conditions of the fountain flow problem according to Hétu et al.[32].

$$\eta(\dot{\gamma},T)=\eta_0\left[1+(\lambda\dot{\gamma})^2\right]^{\left(\frac{n-1}{2}\right)}\beta e^{-\alpha T} \quad , \tag{3}$$

The material used in the simulations is Thermoplastic Polyolefin (TPO) with boundary conditions indicated in Figure 5, and material properties of the casting and rheological model summarized in Table 1.

In order to quantitatively validate these results, the following dimensionless variables are used:

$$x^*=\frac{x}{H_0},\ y^*=\frac{y}{H_0},\ z^*=\frac{z}{Z_0}. \tag{4}$$

Dimensionless time, velocity and temperature are also defined as

$$t^*=t\frac{U_0}{H_0},\ u^*=\frac{u}{U_0},\ T^*=\frac{T-T_w}{T_0-T_w} \tag{5}$$

#### 2.3.3.1 Convergence analysis

Initially, it is relevant to note that most published works using Moldflow® ignore the influence of mesh size. For example, Solanki et al.[33] and Saad et al.[34] recently presented studies addressing design and optimization of molds, respectively, using Moldflow®. Despite the importance of mesh size, mainly in optimization problems, the authors of both works did not discuss the effects of mesh refinement. The authors implicitly assumed that the mesh used in the simulations is refined enough not to significantly influence their results.

There are few examples of mesh size evaluation using Moldflow®. Trad et al.[35] addressed mesh independence by assessing the effect of mesh size in the mold filling time, and concluded that greater accuracy was obtained for refined meshes of size $0.6\,mm$. Miranda and Nogueira[36] experimentally compared the influence of the mesh size in relation to actual injected components, who indicated little variation in the simulated results for mesh sizes smaller than $1.25\,mm$. Marin et al.[37] compared the effect of mesh density in the injection pressure, reaching highest precision in a dual-domain mesh with sizes between 2.0 and $4.0\,mm$. It is worthy to note that the aforementioned mesh sizes are associated with the part or product sizes and shape, especially thickness variations and the presence of free-form shapes. Therefore, one must observe the relative mesh size in order to avoid defining over or under refined meshes. Therefore, the method based on the Richardson extrapolation is a simple tool which will help the mold designer to assess the accuracy of numerical results.

In complex and nonlinear problems, as injection molding, the discretization error (associated with mesh size) is not known *a priori*. In the present work, the Richardson extrapolation technique[38] is applied to estimate the magnitude and order of the discretization error. Richardson extrapolation is based on three progressively refined meshes with a constant refinement ratio. The method assumes that the exact solution for velocities and temperatures, $u^*_{exact}$ and $T^*_{exact}$, can be estimated at any given point $x_i \in R^3$ as

$$u^*_{exact}(x_i) = u^*_h(x_i) + \varepsilon^{u^*}_h = u^*_h(x_i) + \alpha h^{p_h} + O\left(h^{p_h+1}\right), \tag{6}$$

$$T^*_{exact}(x_i) = T^*_h(x_i) + \varepsilon^{T^*}_h = T^*_h(x_i) + \alpha h^{p_h} + O\left(h^{p_h+1}\right), \tag{7}$$

where $u^*_h$ is the discrete solution, $\varepsilon^{u^*}_h$ is the discretization error, $h$ is the mesh size, $\alpha$ is a constant and $p_h$ is the error order. The discretization error and the error order are not known *a priori*. Thus, the Richardson error estimate for dimensionless velocity and temperature, $u^*$ and $T^*$, establishes that the estimated local errors, $\varepsilon^{u^*}_{h_1}$ and $\varepsilon^{T^*}_{h_1}$, and error orders, $\tilde{p}^{u^*}_{h_1}$ and $\tilde{p}^{T^*}_{h_1}$, associated with mesh $h_1$ are

$$\varepsilon^{u^*}_{h_1} = u^*_{exact} - u^*_{h_1} \cong \frac{u^*_{h_1} - u^*_{h_2}}{r^{\tilde{p}} - 1} \quad \text{and} \quad \tilde{p}^{u^*}_{h_1} = \log\left(\frac{u^*_{h_3} - u^*_{h_2}}{u^*_{h_2} - u^*_{h_1}}\right) / \log(r), \tag{8}$$

$$\varepsilon^{T^*}_{h_1} = T^*_{exact} - T^*_{h_1} \cong \frac{T^*_{h_1} - T^*_{h_2}}{r^{\tilde{p}} - 1} \quad \text{and} \quad \tilde{p}^{T^*}_{h_1} = \log\left(\frac{T^*_{h_3} - T^*_{h_2}}{T^*_{h_2} - T^*_{h_1}}\right) / \log(r), \tag{9}$$

where $r = h_3 / h_2 = h_2 / h_1$ is the refinement ratio and $h_1 < h_2 < h_3$ are the mesh sizes.

Richardson's estimate[38] requires meshes with equal refinement rate. Thus, in the present work, the simulations were performed for meshes with a refinement ratio of $r = 2$, ranging from $h = 0.03125\,mm$ to $h = 0.50\,mm$.

## 3. Results and Discussions

This section summarizes the verification study of the computational approach and presents the numerical and experimental comparative study for the filling velocity of the specimen. Firstly, the verification method described in section 2.3.3 for transient flow is presented.

### 3.1 Verification of transient flow

The verification procedure was performed according to the melt polymer transient flow problem proposed by Hétu et al.[32], who also obtained numerical results that will be discussed in this study. The velocity and temperature results at two different injection times were evaluated using the Richardson extrapolation technique[38]. Tables 2 and 3 show the results for velocity and temperature, $u^*$ and $T^*$, corresponding to dimensionless times $t^* = 6.0$ and $t^* = 12.0$, respectively, for a point located at $x^* = 0.50$ and $y^* = 0.50$ for all meshes.

**Table 1.** Material Properties (TPO) and dimensions of Hétu et al.[32].

| Geometric Properties | | | Boundary Conditions | | | Rheological Properties | | |
|---|---|---|---|---|---|---|---|---|
| Parameter | Value | Unit | Parameter | Value | Unit | Parameter | Value | Unit |
| $H_0$ | 1 | mm | $\rho_0$ | 810 | kg·m$^{-3}$ | $\eta_0$ | 3,600 | Pa·s |
| $L_0$ | 10 | mm | $Cp_0$ | 2,500 | J·kg$^{-3}$·K$^{-1}$ | $\lambda$ | 1.62 | s |
| $Z_0$ | 10 | mm | $k_0$ | 0.16 | W·m$^{-1}$·K$^{-1}$ | $n$ | 0.3 | – |
| | | | $U_0$ | 10 | mm·s$^{-1}$ | $\alpha$ | 0.00931 | K$^{-1}$ |
| | | | $T_0$ | 230 | °C | $\beta$ | 1 | – |
| | | | $T_W$ | 50 | °C | | | |

It is observed in Table 2 that the estimated error order $\tilde{p}_{h_1}^{u^*}$ ranges from 1.6408 to 2.0739 for velocity, with an average value $\overline{\tilde{p}}_h^{u^*} = 1.8027$. The "exact" solution determined by Eq. (6) is also indicated in Table 2 as $u^*_{exact} = 1.2088$, while in the study by Hétu et al.[32] is $u^* = 1.1670$. The estimated error order $\tilde{p}_{h_1}^{T^*}$ ranging from 1.6407 to 2.0739 for temperature was also determined, with mean value $\overline{\tilde{p}}_h^{T^*} = 1.8027$. The "exact" solution was $T^*_{exact} = 0.9126$, while in the study by Hétu et al.[32] is $T^* = 0.9050$.

Table 3 shows that, when the flow advances in time at $t^* = 12.0$, the estimated error order $\tilde{p}_{h_1}^{u^*}$ also varies from 1.6408 to 2.0739 for the velocity, with mean value $\overline{\tilde{p}}_h^{u^*} = 1.8027$ with the "exact" solution being $u^*_{exact} = 1.2413$, whereas in the study by Hétu et al.[32] is $u^* = 1.2035$. The estimated error order for temperature $\tilde{p}_{h_1}^{T^*}$ ranges from 1.6407 to 2.0738, with the same mean value $\overline{\tilde{p}}_h^{T^*} = 1.8027$. The "exact" solution was $T^*_{exact} = 0.8702$, whereas in the study by Hétu et al.[32] is $T^* = 0.8645$.

Therefore, the present results obtained using the Moldflow® software indicate that the order of discretization error for both dimensionless velocity and temperature is approximately $\overline{\tilde{p}}_h^{u^*} = \overline{\tilde{p}}_h^{T^*} = 1.8027$, close to the theoretical value of 2.0. Noticeably, this brief evaluation was performed for only one (1) point of the domain ($x^* = 0.50$ and $y^* = 0.50$) and the effects of temporal discretization were not considered. Notwithstanding, this work does not intend to present an in-depth error analysis of mathematical formulations. This "verification" aims to give the reader further quantifiable assurance that present numerical solutions are reliable when compared with the results available in the literature.

### 3.2 Simulated inlet velocity

After the verification step, simulations with Moldfow® software were applied to the specimen model (Figure 3) to capture the filling lines at three different times. The processing and material parameters for the ABS polymer adopted in this study is presented in Miranda et al.[29]. With the results of these lengths, they were applied in Equation 2, whose calculated values can be seen in Table 4.

The results of Table 4 indicate a good agreement in inlet values for velocities obtained in three distinct time steps. Performing an averaging process, the mean value for the inlet velocity obtained with numerical simulation was $\bar{U}_{0sim} = 50.2533\, mm\, s^{-1}$.

### 3.3 Experimental inlet velocity

Under the same simulation conditions, experimental injection tests were performed to measure the flow front lines. The experimental strategy adopted to obtain the flow front was described in details in the work of Miranda et al.[24].

**Table 2.** Dimensionless velocity $u^*$ and temperature $T^*$ ($t^* = 6.0$, $x^* = 0.50$ and $y^* = 0.50$).

| $h$ [mm] | $u^*$ | $\tilde{p}_{h_1}^{u^*}$ | $\varepsilon_{h_1}^{u^*}$ | $u^*_{exact}$ | $T^*$ | $\tilde{p}_{h_1}^{T^*}$ | $\varepsilon_{h_1}^{T^*}$ | $T^*_{exact}$ |
|---|---|---|---|---|---|---|---|---|
| 0.50 | 1.2140 | – | – | – | 0.9179 | – | – | – |
| 0.25 | 1.2101 | – | – | – | 0.9140 | – | – | – |
| 0.125 | 1.2092 | 2.0739 | $-2.8857\times10^{-4}$ | 1.2089 | 0.9131 | 2.0739 | $-2.9218\times10^{-4}$ | 0.9128 |
| 0.0625 | 1.2089 | 1.6937 | $-1.2814\times10^{-4}$ | 1.2088 | 0.9127 | 1.6937 | $-1.2974\times10^{-4}$ | 0.9126 |
| 0.03125 | 1.2088 | 1.6408 | $-4.3354\times10^{-5}$ | 1.2088 | 0.9128 | 1.6407 | $-4.3896\times10^{-5}$ | 0.9126 |

**Table 3.** Dimensionless velocity $u^*$ and temperature $T^*$ ($t^* = 12.0$, $x^* = 0.50$ and $y^* = 0.50$).

| $h$ [mm] | $u^*$ | $\tilde{p}_{h_1}^{u^*}$ | $\varepsilon_{h_1}^{u^*}$ | $u^*_{exact}$ | $T^*$ | $\tilde{p}_{h_1}^{T^*}$ | $\varepsilon_{h_1}^{T^*}$ | $T^*_{exact}$ |
|---|---|---|---|---|---|---|---|---|
| 0.50 | 1.2466 | – | – | – | 0.8755 | – | – | – |
| 0.25 | 1.2426 | – | – | – | 0.8716 | – | – | – |
| 0.125 | 1.2417 | 2.0739 | $-2.9401\times10^{-4}$ | 1.2414 | 0.8707 | 2.0738 | $-2.8670\times10^{-4}$ | 0.8704 |
| 0.0625 | 1.2414 | 1.6937 | $-1.3056\times10^{-4}$ | 1.2413 | 0.8704 | 1.6937 | $-1.2731\times10^{-4}$ | 0.8702 |
| 0.03125 | 1.2413 | 1.6408 | $-4.4170\times10^{-5}$ | 1.2412 | 0.8703 | 1.6407 | $-4.3072\times10^{-5}$ | 0.8702 |

**Table 4.** Line measurements and calculated inlet velocity with the respective standard deviations in the simulated results.

| Lines | Δt = 0.10 s | | Δt = 0.20 s | | Δt = 0.30 s | |
|---|---|---|---|---|---|---|
| $\Delta x_1$ (mm) | 4.89 | | 9.76 | | 14.56 | |
| $\Delta x_2$ (mm) | 5.03 | | 10.04 | | 14.98 | |
| $\Delta x_3$ (mm) | 5.06 | | 10.10 | | 15.07 | |
| $\Delta x_4$ (mm) | 5.13 | | 10.23 | | 15.27 | |
| $\Delta x_5$ (mm) | 5.10 | | 10.17 | | 15.18 | |
| $\overline{\Delta x}$ *(mm)* | 5.042 | ± 0.0931 | 10.060 | ± 0.1823 | 15.012 | ± 0.2754 |
| **Calculated Velocities** | | | | | | |
| $\bar{U}_{0sim}$ **(mm·s$^{-1}$)** | **50.42** | ± 0.9311 | **50.30** | ± 0.9117 | **50.04** | ± 0.9182 |

**Table 5.** Line measurements and calculated initial velocity with the respective standard deviations in the experimental results.

| Lines | Δt = 0.10 s | | Δt = 0.20 s | | Δt = 0.30 s | |
|---|---|---|---|---|---|---|
| $\Delta x_1$ (mm) | 4.95 | | 9.88 | | 14.75 | |
| $\Delta x_2$ (mm) | 5.01 | | 10.01 | | 14.94 | |
| $\Delta x_3$ (mm) | 5.03 | | 10.03 | | 14.97 | |
| $\Delta x_4$ (mm) | 5.09 | | 10.16 | | 15.16 | |
| $\Delta x_5$ (mm) | 5.06 | | 10.10 | | 15.07 | |
| $\overline{\Delta x}$ *(mm)* | 5.028 | ± 0.0531 | 10.036 | ± 0.1055 | 14.978 | ± 0.1542 |
| **Calculated Velocities** | | | | | | |
| $\bar{U}_{0sim}$ **(mm·s⁻¹)** | **50.28** | ± 0.5310 | **50.18** | ± 0.5275 | **49.9267** | ± 0.5139 |

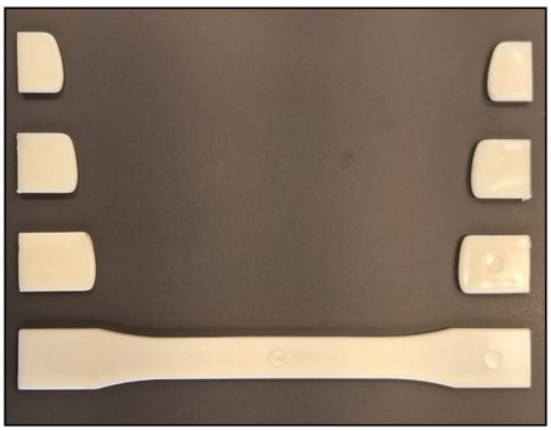

**Figure 6.** Advancement of the flow front during filling stage in the experimental process with an interval of $\Delta t = 0.1 s$, $\Delta t = 0.2 s$, $\Delta t = 0.3 s$ and the cavity is completely filled.

Noticeably, the inertia of the injection screw was not accounted for explicitly; however, its effects are included in the measurements of the flow front at the injected part. The development of the flow front after solidification can be seen in Figure 6.

Figure 6 illustrates that, in the beginning of the filling front, the inlet velocity of the molten polymer is non-linear and asymmetrical, that is, due to the injection channel being displaced and flowing on only one side before reaching the cavity. This displacement causes the molten polymer to pass the gate with a greater velocity on one side of the cavity than on the other. The length values shown in Table 5 represent an average of ten injection samples at each instant of time for performing the calculations.

The values collected experimentally in Table 5 indicate that an average injection velocity of $\bar{U}_{exp} = 50.1289\, mm\, s^{-}$ is sufficiently favourable. In summary, although the experimentally calculated inlet velocity reached a value lower than the simulated one, the difference between the values is approximately $0.1244\, mm\, s^{-1}$ (less than 1%), which is considerably small considering an injection problem.

## 4. Conclusions

Proper control of the gate inlet velocity in thermoplastic injection molds is essential to obtain products with desired characteristics, avoiding defects and ensuring process efficiency. This work presents a numerical and experimental approaches on how to determine the entry velocity in thermoplastic injection molds and a mesh convergence study using the Moldflow® simulation software. The following points highlight the discussions:

- Verification of the GHS numerical model was performed based on the injection mold problem proposed by Hétu et al.[32]. The error magnitude and order were found acceptable, with error order for velocity and temperature around 1.8, close to the theoretical value of 2.0;
- Experimental and numerical methodologies for capturing the gate inlet velocity directly in the cavities of injection molds were addressed. Assessment of the inlet velocity based on both strategies shows differences smaller than 1%;
- The proposed strategy to determine the gate inlet velocity makes it possible to simulate the injection molding processes without including the injection channel, thereby reducing the simulation time.

It is relevant to note that the design engineer who is able to understand and anticipate the gate inlet velocity in the simulations will be able to optimize simulations in thermoplastic injection molds of parts with complex geometries, thereby guaranteeing the production of high-quality polymer parts, with good dimensional accuracy, strength and suitable surface finish.

## 5. Author's Contribution

- **Conceptualization –** Diego Alves de Miranda.
- **Data curation –** Diego Alves de Miranda; Willian Kévin Rauber.
- **Formal analysis –** Diego Alves de Miranda; Willian Kévin Rauber.
- **Funding acquisition –** NA.
- **Investigation –** Diego Alves de Miranda; Willian Kévin Rauber; Paulo Sergio Berving Zdanski; Miguel Vaz Jr.
- **Methodology –** Diego Alves de Miranda; Willian Kévin Rauber; Paulo Sergio Berving Zdanski; Miguel Vaz Jr.
- **Project administration –** Paulo Sergio Berving Zdanski.

- **Resources –** NA.
- **Software –** Diego Alves de Miranda; Willian Kévin Rauber.
- **Supervision –** Paulo Sergio Berving Zdanski; Miguel Vaz Jr.
- **Validation –** Diego Alves de Miranda; Miguel Vaz Jr.
- **Visualization –** Diego Alves de Miranda; Willian Kévin Rauber.
- **Writing – original draft –** Diego Alves de Miranda; Willian Kévin Rauber; Miguel Vaz Jr; Paulo Sergio Berving Zdanski.
- **Writing – review & editing –** Diego Alves de Miranda; Willian Kévin Rauber; Miguel Vaz Jr; Paulo Sergio Berving Zdanski.

## 6. Acknowledgements

The second author thanks the "State University of Santa Catarina (UDESC) – Program for Postgraduate Tutoring Scholarship (PROMOP)". The second, third, fourth and last authors acknowledge the "Research and Innovation Support Foundation of the State of Santa Catarina (FAPESC)", Finance Code 2023TR000563, and the last author thanks the financial support provided by the Brazilian "National Council for Scientific and Technological Development (CNPq)" under grant 306821/2021-4.

## 7. References

1. Krantz, J., Nieduzak, Z., Kazmer, E., Licata, J., Ferki, O., Gao, P., Sobkowicz, M. J., & Masato, D. (2023). Investigation of pressure-controlled injection molding on the mechanical properties and embodied energy of recycled high-density polyethylene. *Sustainable Materials and Technologies*, *36*, e00651. http://dx.doi.org/10.1016/j.susmat.2023.e00651.
2. Tsou, H.-H., Huang, C.-C., Zhao, T.-W., & Wang, Z.-H. (2022). Design and validation of sensor installation for online injection molding sidewall deformation monitoring. *Measurement*, *205*, 112200. http://dx.doi.org/10.1016/j.measurement.2022.112200.
3. Bianchi, M. F., Gameros, A. A., Axinte, D. A., Lowth, S., Cendrowicz, A. M., & Welch, S. T. (2021). Regional temperature control in ceramic injection moulding: an approach based on cooling rate optimization. *Journal of Manufacturing Processes*, *68*, 1767-1783. http://dx.doi.org/10.1016/j.jmapro.2021.06.069.
4. Fu, J., Zhang, X., Quan, L., & Ma, Y. (2022). Concurrent structural topology and injection gate location optimization for injection molding multi-material parts. *Advances in Engineering Software*, *165*, 103088. http://dx.doi.org/10.1016/j.advengsoft.2022.103088.
5. He, H., Xing, Y., Wang, R., Lu, Y., Zhang, L., & Li, F. (2023). Optimization design of cooling system for injection molding mold of non-pneumatic tire. *Thermal Science and Engineering Progress*, *42*, 101866. http://dx.doi.org/10.1016/j.tsep.2023.101866.
6. Marques, S., Souza, A. F., Miranda, J., & Yadroitsau, I. (2015). Design of conformal cooling for plastic injection moulding by heat transfer simulation. *Polímeros: Ciência e Tecnologia*, *25*(6), 564-574. http://dx.doi.org/10.1590/0104-1428.2047.
7. Baum, M., Jasser, F., Stricker, M., Anders, D., & Lake, S. (2022). Numerical simulation of the mold filling process and its experimental validation. *International Journal of Advanced Manufacturing Technology*, *120*(5), 3065-3076. http://dx.doi.org/10.1007/s00170-022-08888-9.
8. Chai, B. X., Eisenbart, B., Nikzad, M., Fox, B., Blythe, A., Blanchard, P., & Dahl, J. (2021). Simulation-based optimisation for injection configuration design of liquid composite moulding processes: a review. *Composites. Part A, Applied Science and Manufacturing*, *149*, 106540. http://dx.doi.org/10.1016/j.compositesa.2021.106540.
9. Zhang, Y., Liu, F., Huang, Z., Xie, X., Shan, B., & Zhou, H. (2015). Dispersed phase deformation modeling of immiscible polymer blends in injection molding. *Advances in Polymer Technology*, *34*(4), 21515. http://dx.doi.org/10.1002/adv.21515.
10. Morak, M., Tscharnuter, D., Lucyshyn, T., Hahn, W., Göttlinger, M., Kummer, M., Steinberger, R., & Gross, T. (2018). Optimization of fiber prediction model coefficients in injection molding simulation based on micro computed tomography. *Polymer Engineering and Science*, *52*(2), 152-160. http://dx.doi.org/10.1002/pen.25013.
11. Onken, J., Verwaayen, S., & Hopmann, C. (2020). Evaluation of healing models to predict the weld line strength of the amorphous thermoplastic polystyrene by injection molding simulation. *Polymer Engineering and Science*, *61*(3), 754-766. http://dx.doi.org/10.1002/pen.25614.
12. Gruber, P. A., & Miranda, D. A. (2020). Heat transfer simulation for decision making in plastic injection mold design. *Polímeros: Ciência e Tecnologia*, *30*(1), e2020005. http://dx.doi.org/10.1590/0104-1428.08319.
13. Cao, W., Shen, Y., Wang, P., Yang, H., Zhao, S., & Shen, C. (2019). Viscoelastic modeling and simulation for polymer melt flow in injection/compression molding. *Journal of Non-Newtonian Fluid Mechanics*, *274*, 104186. http://dx.doi.org/10.1016/j.jnnfm.2019.104186.
14. Xu, X., & Yu, P. (2017). Modeling and simulation of injection molding process of polymer melt by a robust SPH method. *Applied Mathematical Modelling*, *48*, 384-409. http://dx.doi.org/10.1016/j.apm.2017.04.007.
15. Marion, S., Sardo, L., Joffre, T., & Pigeonneau, F. (2023). First steps of the melting of an amorphous polymer through a hot-end of a material extrusion additive manufacturing. *Additive Manufacturing*, *65*, 103435. http://dx.doi.org/10.1016/j.addma.2023.103435.
16. Young, W.-B. (2017). Lattice Boltzmann simulation of polymer melt flow with a low Reynolds number. *International Journal of Heat and Mass Transfer*, *115*, 784-792. http://dx.doi.org/10.1016/j.ijheatmasstransfer.2017.08.080.
17. Zdanski, P. S. B., & Vaz, M., Jr. (2011). A numerical method for simulation of incompressible three-dimensional newtonian and non-newtonian flows. *Numerical Heat Transfer Part B*, *59*(5), 360-380. http://dx.doi.org/10.1080/10407790.2011.572727.
18. Tutar, M., & Karakus, A. (2014). Numerical study of polymer melt flow in a three-dimensional sudden expansion: viscous dissipation effects. *Journal of Polymer Engineering*, *34*(8), 755-764. http://dx.doi.org/10.1515/polyeng-2013-0273.
19. Gao, P. (2022). Three dimensional finite element computation of the non-isothermal polymer filling process by the phase field model. *Advances in Engineering Software*, *172*, 103207. http://dx.doi.org/10.1016/j.advengsoft.2022.103207.
20. Fernandes, C., Pontes, A. J., Viana, J. C., & Gaspar-Cunha, A. (2016). Modeling and optimization of the injection-molding process: a review. *Advances in Polymer Technology*, *37*(2), 429-449. http://dx.doi.org/10.1002/adv.21683.
21. Liao, T., Zhao, X., Yang, X., Whiteside, B., Coates, P., Jiang, Z., & Men, Y. (2019). Predicting the location of weld line in microinjection-molded polyethylene via molecular orientation distribution. *Journal of Polymer Science. Part B, Polymer Physics*, *57*(24), 1705-1715. http://dx.doi.org/10.1002/polb.24905.

22. Mourya, A., Nanda, A., Parashar, K., Sushant, & Kumar, R. (2022). An explanatory study on defects in plastic molding parts caused by machine parameters in injection molding process. *Materials Today: Proceedings*, *78*(Pt 3), 656-661. http://dx.doi.org/10.1016/j.matpr.2022.12.070.
23. Corazza, E. J., Sacchelli, C. M., & Marangoni, C. (2012). Cycle time reduction of thermoplastic injection using nitriding treatment surface molds. *Información Tecnológica*, *23*(3), 51-58. http://dx.doi.org/10.4067/S0718-07642012000300007.
24. Miranda, D. A., Rauber, W. K., Vaz, M., Jr., Alves, M. V. C., Lafratta, F. H., Nogueira, A. L., & Zdanski, P. S. B. (2023). Analysis of numerical modeling strategies to improve the accuracy of polymer injection molding simulations. *Journal of Non-Newtonian Fluid Mechanics*, *315*, 105033. http://dx.doi.org/10.1016/j.jnnfm.2023.105033.
25. Gim, J., & Turng, L.-S. (2022). A review of current advancements in high surface quality injection molding: measurement, influencing factors, prediction, and control. *Polymer Testing*, *115*, 107718. http://dx.doi.org/10.1016/j.polymertesting.2022.107718.
26. Hentati, F., Hadriche, I., Masmoudi, N., & Bradai, C. (2020). Experimental design to enhance the surface appearance, the internal structure, and the shear stresses of injected and metallized polycarbonate/acrylonitrile–butadiene-styrene parts. *Journal of Applied Polymer Science*, *137*(7), 48384. http://dx.doi.org/10.1002/app.48384.
27. Yu, S., Kong, W., Xu, L., Zou, J., Han, W., Liu, Z., Luo, J., Xie, Z., Wu, H., & Zhou, H. (2023). Cellular distribution and warpage deformation in double-sided in-mold decoration combined with microcellular injection molding process. *Journal of Materials Processing Technology*, *317*, 117982. http://dx.doi.org/10.1016/j.jmatprotec.2023.117982.
28. Acrylonitrile Butadiene Styrene – ABS. (2010). ABS –750 - Data Sheet of Acrylonitrile Butadiene Styrene. South Korea: Kumho Petrochemical.
29. Miranda, D. A., Rauber, W. K., Vaz, M., Jr., Nogueira, A. L., Bom, R. P., & Zdanski, P. S. B. (2023). Evaluation of the predictive capacity of viscosity models in polymer melt filling simulations. *Journal of Materials Engineering and Performance*, *32*(4), 1707-1720. http://dx.doi.org/10.1007/s11665-022-07200-w.
30. Marin, F., Souza, A. F., Ahrens, C. H., & Lacalle, L. N. L. (2021). A new hybrid process combining machining and selective laser melting to manufacture an advanced concept of conformal cooling channels for plastic injection molds. *International Journal of Advanced Manufacturing Technology*, *113*(5), 1561-1576. http://dx.doi.org/10.1007/s00170-021-06720-4.
31. Kennedy, P. K. (2008). *Practical and scientific aspects of injection molding simulation* (Doctoral thesis). Technische Universiteit Eindhoven, Eindhoven, Netherlands. http://dx.doi.org/10.6100/IR634914.
32. Hétu, J.-F., Gao, D. M., Garcia-Rejon, A., & Salloum, G. (1998). 3D finite element method for the simulation of the filling stage in injection molding. *Polymer Engineering and Science*, *38*(2), 223-236. http://dx.doi.org/10.1002/pen.10183.
33. Solanki, B. S., Singh, H., & Sheorey, T. (2022). Towards an accurate pressure estimation in injection molding simulation using surrogate modeling. *International Journal on Interactive Design and Manufacturing*, *16*(4), 1615-1632. http://dx.doi.org/10.1007/s12008-022-00887-0.
34. Saad, S., Sinha, A., Cruz, C., Régnier, G., & Ammar, A. (2022). Towards an accurate pressure estimation in injection molding simulation using surrogate modeling. *International Journal of Material Forming*, *15*(6), 72. http://dx.doi.org/10.1007/s12289-022-01717-0.
35. Trad, M. A. B., Demers, V., Côté, R., Sardarian, M., & Dufresne, L. (2020). Numerical simulation and experimental investigation of mold filling and segregation in low-pressure powder injection molding of metallic feedstock. *Advanced Powder Technology*, *31*(3), 1349-1358. http://dx.doi.org/10.1016/j.apt.2020.01.018.
36. Miranda, D. A., & Nogueira, A. L. (2019). Simulation of an injection process using a CAE tool: assessment of operational conditions and mold design on the process efficiency. *Materials Research*, *22*(2), e20180564. http://dx.doi.org/10.1590/1980-5373-mr-2018-0564.
37. Marin, F., Souza, A. F., Pabst, R. G., & Ahrens, C. H. (2019). Influences of the mesh in the CAE simulation for plastic injection molding. *Polímeros*, *29*(3), e2019043. http://dx.doi.org/10.1590/0104-1428.05019.
38. Richardson, L. F. (1911). The approximate arithmetical solution by finite differences of physical problems involving differential equations with an application to the stresses in a masonary dam. *Philosophical Transactions of the Royal Society of London. Series A, Containing Papers of a Mathematical or Physical Character*, *210*(459-470), 307-357. http://dx.doi.org/10.1098/rsta.1911.0009.


*Received: Nov. 13, 2023*
*Revised: Feb. 26, 2024*
*Accepted: Mar. 05, 2024*